

Statistical Shape Modeling of Cam Femoroacetabular Impingement

Michael D. Harris,^{1,2,3} Manasi Datar,^{3,4} Ross T. Whitaker,^{1,3,4} Elizabeth R. Jurrus,³ Christopher L. Peters,² Andrew E. Anderson^{1,2,3,5}

¹Department of Bioengineering, University of Utah, Salt Lake City, Utah, ²Department of Orthopaedics, 590 Wakara Way A-100, Salt Lake City, Utah, 84107, ³Scientific Computing and Imaging Institute, University of Utah, Salt Lake City, Utah, ⁴School of Computing, University of Utah, Salt Lake City, Utah, ⁵Department of Physical Therapy, University of Utah, Salt Lake City, Utah

Received 3 October 2012; accepted 23 April 2013

Published online 7 July 2013 in Wiley Online Library (wileyonlinelibrary.com). DOI 10.1002/jor.22389

ABSTRACT: Statistical shape modeling (SSM) was used to quantify 3D variation and morphologic differences between femurs with and without cam femoroacetabular impingement (FAI). 3D surfaces were generated from CT scans of femurs from 41 controls and 30 cam FAI patients. SSM correspondence particles were optimally positioned on each surface using a gradient descent energy function. Mean shapes for groups were defined. Morphological differences between group mean shapes and between the control mean and individual patients were calculated. Principal component analysis described anatomical variation. Among all femurs, the first six modes (or principal components) captured significant variations, which comprised 84% of cumulative variation. The first two modes, which described trochanteric height and femoral neck width, were significantly different between groups. The mean cam femur shape protruded above the control mean by a maximum of 3.3 mm with sustained protrusions of 2.5–3.0 mm along the anterolateral head-neck junction/distal anterior neck. SSM described variations in femoral morphology that corresponded well with areas prone to damage. Shape variation described by the first two modes may facilitate objective characterization of cam FAI deformities; variation beyond may be inherent population variance. SSM could characterize disease severity and guide surgical resection of bone. © 2013 Orthopaedic Research Society. Published by Wiley Periodicals, Inc. *J Orthop Res* 31:1620–1626, 2013

Keywords: hip; statistical shape modeling; femoroacetabular impingement; cam

Femoroacetabular impingement (FAI) is caused by reduced clearance between the femoral head and acetabulum due to anatomic abnormalities of the femur (cam FAI), acetabulum (pincer FAI), or both (mixed FAI).¹ Cam FAI is characterized by an aspherical femoral head or reduced femoral head-neck offset. During hip flexion, the abnormally shaped femur may cause shearing at the chondrolabral junction thereby damaging articular cartilage and the acetabular labrum.²

Currently, diagnosis of cam FAI is largely accomplished using 2D measurements of femur morphology acquired from radiographic projections or a series of radial planes from CT or MR images.^{3–5} 2D measures provide initial diagnosis of cam FAI, but their reliability has been debated.^{6,7} Also, no agreement exists on the range of measurements that should be considered normal.^{8–10} Furthermore, radiographic measures give only a limited description of femoral anatomy or shape variation among cam FAI deformities. Together, these limitations translate into a high misdiagnosis rate. In a series of FAI patients treated in our clinic, 40% had seen multiple providers, and 15% had undergone surgery unrelated to the hip joint (e.g., hernia).¹¹

3D femur reconstructions from CT images can visualize the entire femoral head. However, evaluations of cam FAI using 3D reconstructions have relied on the assumption that a sphere is the ideal head shape.^{12,13} In contrast, statistical shape modeling

(SSM) can be applied to 3D reconstructions to objectively compare complex morphology without idealizing underlying geometry.^{14,15} Prior orthopaedic applications of SSM have included analyses of tibiofemoral and patellofemoral joints and methods to reconstruct femur or pelvis shape from sparse image data.^{16–22} Most SSM strategies distribute a labeled set of points across representative shapes for a given population.^{14,15} Methods of point placement may involve manual placement at anatomic landmarks, derivation from finite element meshes, or automatic placement based on point-to-point minimization of distance and entropy.^{14,18,23} Regardless of the method, by optimizing and comparing the positional configurations of the labeled points, SSM can quantify and visualize geometric variation within the population.

Applying SSM to study cam FAI may improve diagnosis and pre-operative planning. SSM can be applied to reconstructions of cam FAI and healthy femurs to generate 3D representatives of the average cam FAI femur compared to the average control. SSM also facilitates analysis of shape variations among femurs, which may have clinical use in describing the spectrum of cam deformities and classifying the deformity severity on a patient-specific basis.

We generated 3D reconstructions of femoral heads from CT images and applied SSM to quantify variation and morphologic differences between femurs with and without cam FAI.

METHODS

Subject Selection

A cohort of cam FAI patients was retrospectively collected from the University of Utah and Intermountain Healthcare orthopaedic centers. Subject selection and modeling received IRB approval from both institutions. Volumetric CT images of the pelvis and proximal femur were retrospectively

Grant sponsor: NIH; Grant numbers: R01AR05344, P41RR012553-14, P41GM103545-14; Grant sponsor: NIH/NCBC National Alliance for Medical Image Computing; Grant number: U54-EB005149; Grant sponsor: NSF; Grant number: CCF-073222.

Correspondence to: Andrew E. Anderson (T: 801-587-5208, F: 801-587-5211; E-mail: andrew.anderson@hsc.utah.edu)

© 2013 Orthopaedic Research Society. Published by Wiley Periodicals, Inc.

acquired from 30 cam FAI patients (28 males, 2 females). All patients had presented with hip and groin pain during activity, tested positive during a clinical impingement exam, showed radiographic evidence of a cam lesion and/or reduced head-neck offset, and were scheduled for hip preservation surgery to address cam FAI. Sixteen image sets had been acquired using a Siemens SOMATOM 128 Definition CT Scanner (120 kVp tube voltage, 512×512 acquisition matrix, 1.0 mm slice thickness, 0.9–1.0 pitch, 250 mAs + CareDose tube current, 300–400 mm field-of-view) as part of a previous study. The remaining 14 image sets were acquired as part of standard patient care using a GE LightSpeed VCT scanner (120 kVp, 512×512 , 0.625 slice thickness, 1.0 pitch, 135 mAs, ~ 230 mm field-of-view).

CT scans for 79 possible control femurs were retrospectively obtained (with IRB approval). Of these, 20 subjects received a CT arthrogram as part of a previous study²⁴ using the scanner and settings listed above. These subjects had no history of hip pain and no radiographic evidence of OA as assessed by a senior musculoskeletal radiologist. The remaining 59 femurs were from a database of cadavers that had been previously scanned. Prior to scanning, each cadaveric femur was aligned in an anatomic neutral position.²⁵ Images were acquired using a GE High Speed CTI Single Slice Helical CT Scanner (100 kVp tube voltage, 512×512 acquisition matrix, 1.0 mm slice thickness, 1.0 pitch, 100 mAs tube current, 160 mm field of view).

Digitally reconstructed radiographs (DRR) were generated from the images to simulate a standing frog-leg lateral x-ray, with the femur flexed $\sim 35^\circ$ and externally rotated $\sim 60^\circ$. Radiographic description of head shape was completed for all patients and possible controls by measuring the alpha angle and head neck offset described by Notzli et al. and Eijer et al., respectively, and adapted by Clohisy et al. for the frog-leg lateral view (Fig. 1).^{26–28} Femurs with an alpha angle $< 55.5^\circ$ and head-neck offset > 7 mm were included as controls.^{2,8} Inclusion of femurs as controls was also based on gross screening for cartilage damage and bony abnormalities. Thirty-eight control femurs were excluded, leaving 41 femurs (29 males, 12 females; 15 live, 26 cadaveric).

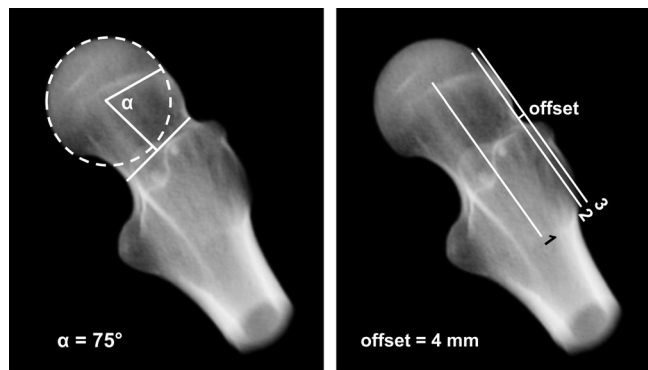


Figure 1. Alpha angle and head-neck offset for a cam FAI patient, measured from the standing frog-leg lateral view. Left—A circle was fit to the head and a line was drawn across the narrow section of the neck. Alpha angle (α) was measured between a line from the center of the neck to the head center and a second line from the head center to the point where the femur deviated from the best-fit circle. Right—Head-neck offset was measured by drawing line 1 along the neck axis, line 2 parallel to line 1 and tangent to the anterolateral neck, and line 3 parallel to line 1 tangent to the anterolateral head. Offset was measured as the distance lines 2 and 3. Adapted from Harris et al.³⁴

3D Reconstruction and SSM Preprocessing

The proximal femur to lesser trochanter of each femur was segmented and reconstructed from the CT image data using Amira (v5.4, Visage Imaging, San Diego, CA) and validated threshold settings.²⁹ To improve resolution of the segmentation mask, images were up-sampled to $0.22 \text{ mm} \times 0.22 \text{ mm} \times 0.33 \text{ mm}$.²⁴ Reconstructed surfaces were triangulated, and segmentation artifacts were removed by slightly smoothing surfaces using tools available in Amira. Reconstructions were cropped at the superior aspect of the lesser trochanter, considered to be the most inferior location where cam FAI deformities might extend. The cropped reconstructions were then aligned in Amira using a built-in iterative closest point algorithm to minimize the root mean square (RMS) distance between surfaces. Finally, surface reconstructions were converted to binary segmentations in a uniform bounding box of size $512 \times 512 \times 512$, with an isotropic voxel resolution of $0.24 \text{ mm} \times 0.24 \text{ mm} \times 0.24 \text{ mm}$.

Statistical Shape Modeling

A basic principle of most SSMs is to place particles at corresponding locations on every shape in the population of interest. Optimization routines, designed to minimize descriptive length or entropy, seek to establish particle configurations that conform qualitatively to the anatomy of individuals and capture underlying shape variability in the population as a whole. We used the correspondence methods of Cates et al.¹⁴ and Datar et al.,³⁰ which employ a variational formulation of ensemble entropy to optimize particle positioning. Compared to other SSM methods that rely on relatively few manually placed landmarks or the necessity for training shapes, the SSM techniques of Cates et al. provide a geometrically accurate sampling of individual femurs, while computing a statistically simple model of the ensemble.¹⁴ Consequently, the number of correspondence particles and the ensemble size can be increased without large computational expense. Particle initialization is performed automatically, which eliminates error that may be introduced by manually placing particles at anatomic landmarks. These methods have been implemented in the ShapeWorks software (<http://www.sci.utah.edu/software/shapeworks.html>) and were used to conduct the statistical shape analysis.

Binary segmentations of the femurs were output from Amira, preprocessed to remove aliasing artifacts, and 2,048 particles were placed on each femur, using an iterative, hierarchical splitting strategy (Fig. 2). This strategy proceeded by randomly choosing a surface location and there placing a single particle that was then split to produce a second, nearby particle. Initial locations of the two particles were determined using a system of repulsive forces until a steady state between the particles was achieved. The splitting process and steady state initialization were repeated until 2,048 particles were placed on each surface. Thus, the initialization proceeded simultaneously with a preliminary steady state optimization in a multi-scale fashion, generating progressively more detailed correspondence models with each split.

The initial particle correspondences were further optimized using a gradient descent approach with a cost function that produced a compact distribution of samples in shape space, while providing uniformly-distributed particle positions on the femur surfaces to achieve a faithful shape representation. The generalized Procrustes algorithm was applied regularly during optimization to align shapes with respect to rotation and translation and to normalize with respect to scale.³¹ Group labels were used to separate the particle configurations of

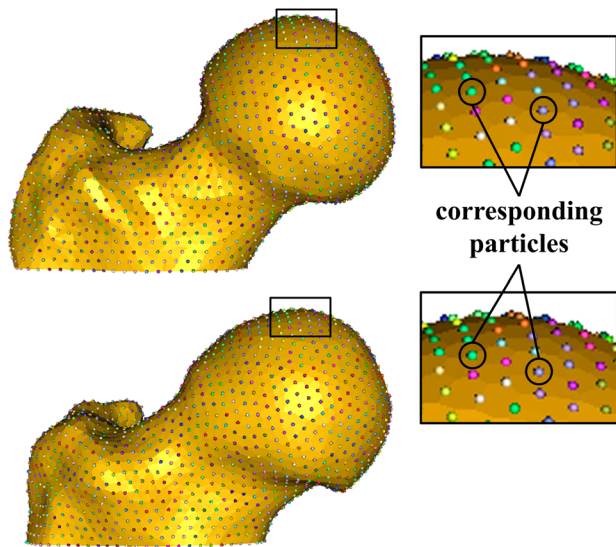


Figure 2. Correspondence particle distribution with 2,048 particles on a control (top) and cam FAI (bottom) femur.

controls and cam patients, and the mean shape for each group was constructed as the mean of the particle configurations from all shapes belonging to that group.

Analysis

Demographic and radiographic measurements were tested for significant differences between control and patient groups using the Mann–Whitney rank sum test. A Hotelling T^2 test was used to test for group differences between the mean control and patient shapes, with the null hypothesis that the two groups were drawn from the same distribution. Morphological differences were then calculated as the distance between mean shapes or between the control mean and individual cam patients. Principal component analysis (PCA) was used to reduce high-dimensional SSM correspondence data to a smaller set of linearly uncorrelated components (i.e., modes) that describe the variation existing within the ensemble of femur shapes. Principal component loading

values (i.e., PC scores) were determined for all femurs, and parallel analysis was used to determine the number of modes containing non-spurious, or significant, shape variation.³² Application of parallel analysis prevented the under-extraction (i.e., loss of meaningful information) or over-extraction (i.e., inclusion of random noise) in the shape variation analysis. Principal component loading values were compared between control and patient groups for modes found to contain significant information using Student's T -test with a Finner's adjustment for multiple comparisons.³³ PCA was then applied to the control and patient groups separately to determine major intra-group variations.

Shape variation (PC loading values) was correlated with existing 2D and 3D measures of femoral anatomy using Pearson's correlation coefficient. First, PC loading values were correlated with 2D alpha angle and head-neck offset measurements. Next, native 3D reconstructions of each head were isolated from the femur at the head-neck junction and fit to a sphere. Maximum deviations were then measured as the distance between the native head and the corresponding best-fit sphere.³⁴ Maximum deviations were then correlated with PC loading values, alpha angles, and head-neck-offsets.

RESULTS

The average and standard deviation age, weight, height, and BMI of the patients and (controls) were 27 ± 8 (31 ± 10) years, 84 ± 15 (80 ± 18) kg, 181 ± 8 (177 ± 8) cm, and 25.6 ± 4.3 (25.4 ± 5.5) kg/m², respectively. Alpha angles and head-neck offsets of the patients and (controls) were 68.4 ± 15.6 (43.0 ± 5.2)° and 4.4 ± 1.7 (7.8 ± 1.1) mm, respectively. Age, weight, and BMI values were not different between controls and patients ($p \geq 0.105$), whereas alpha angles and head-neck offsets were different between the groups ($p < 0.001$).

The Hotelling T^2 test demonstrated significant differences between the patient and control mean shapes ($p < 0.001$). Morphologically, the patient mean shape protruded above the control mean by a maximum of 3.3 mm in the anterolateral head-neck junction (Fig. 3).

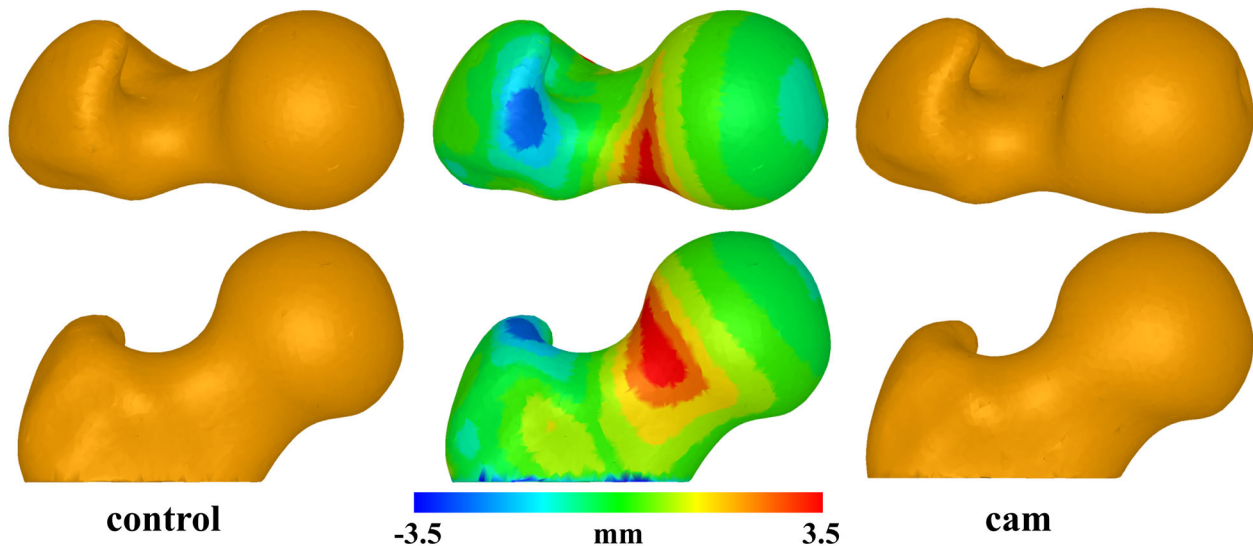


Figure 3. Mean control (left) and cam (right) shapes. Middle images demonstrate how the mean cam shape differed relative to the mean control shape (shown). Top and bottom rows show different rotations of the femoral head.

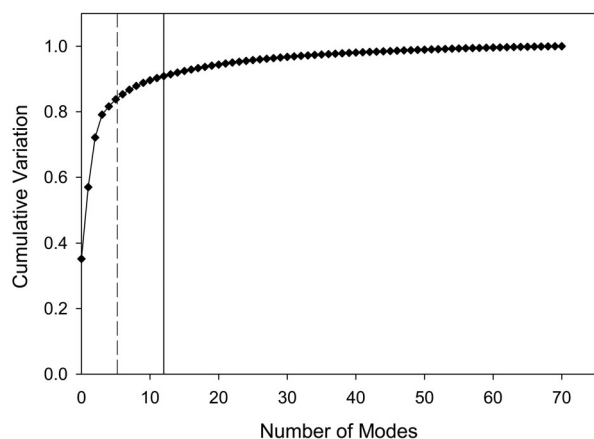


Figure 4. Cumulative shape variation captured in the 70 PCA modes when PCA was run for all femurs. Ninety percent of the variation was captured in the first 12 modes (vertical solid line), while significant variations were captured in the first six modes (vertical dashed line).

Sustained protrusions of ~ 2.5 – 3.0 mm were distributed from the AP midline of the femoral neck along the anterolateral head–neck junction and distally along the anterior neck. Maximum deviations between individual patient femur shapes and the mean control shape were primarily in the anterosuperior to anterolateral head–neck junction, and ranged between 2.3 and 8.3 mm.

The first 12 modes captured 90% of the cumulative variation among femurs (Fig. 4). However, parallel analysis determined that the first six modes captured significant (non-spurious) variation and were used for further analysis. The six modes captured 83.8% of the cumulative variation among all femurs. Specifically, mode 1 captured 35.2% of the variation, followed by mode 2 at 21.8%, mode 3 at 15.2%, mode 4 at 6.9%,

mode 5 at 2.5%, and mode 6 at 2.2% of the variation. PC loading values between controls and patients were significant ($p < 0.001$) for the first two modes.

PCA, run on the control and patient groups independently, showed similar areas of intra-group variation. Qualitative and quantitative descriptions of variation captured by the first three modes are shown in Figure 5. For both groups, variation in mode 1 was most substantial at the femoral offset (i.e., medial-lateral distance from tip of greater trochanter to center of the head) and the distance between the proximal tip of the greater trochanter and the proximal lesser trochanter. For the patient group, mode 1 also captured variation in concavity at the head–neck junction. For both groups, mode 2 primarily described variation in the diameter of the neck. Finally, mode 3 captured variation in the curvature of the greater trochanter in both groups.

Correlations of alpha angles and head-neck offsets with PC loading values from the first four modes were moderate to weak. Pearson's correlation coefficients for alpha angles and (head-neck offsets) with PC loadings were $r = 0.407$ (-0.303), 0.357 (-0.391), and 0.137 (0.014) for modes 1, 2, and 3, respectively.

Maximum deviations from best-fit spheres were 1.95 ± 0.61 mm for the control subjects and 4.79 ± 1.54 mm for patient femurs. Maximum deviations were different between patients and controls ($p < 0.001$). Correlations between maximum deviation and PC loading values were moderate to weak, with Pearson's correlation coefficients of $r = 0.433$, 0.360 , and 0.168 for modes 1, 2, and 3, respectively. Correlations between radiographic measurements and maximum deviations were $r = 0.863$ (alpha angle) and $r = -0.781$ (head–neck offset).

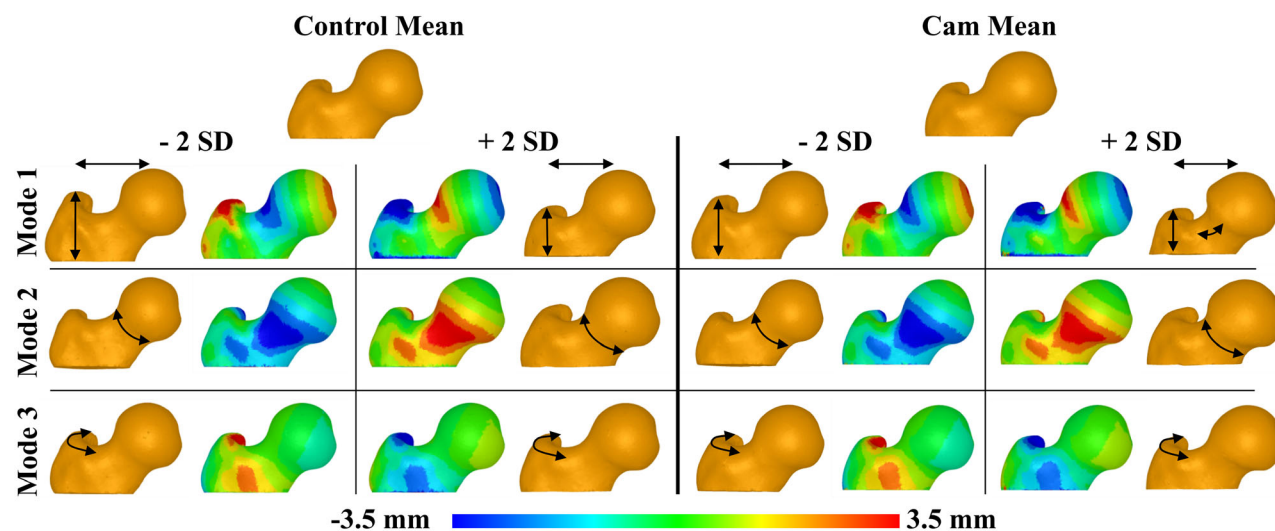


Figure 5. Shape variation captured in the first three modes. PCA was run independently on the control and patient femur groups. Shapes are shown at ± 2 SD from the mean for each group in each mode. Color plots indicate differences between mean shapes and ± 2 SD shapes, with respect to the mean shape. Arrows qualitatively show areas of greatest variation captured by each mode. Plots of differences between mean and standard deviation shapes were similar between controls and patients. However, for mode 1, the concavity in the $+2$ SD shape was substantially different between patients (arrow) and controls (no arrow).

DISCUSSION

We used SSM to quantify and compare femoral head morphology between control and cam FAI femurs. A primary result was the computation of mean femoral shapes for controls and cam FAI patients. The greatest differences between the mean shapes were located along the anterolateral head–neck junction, corresponding well with the locations of cam lesions and corresponding joint damage in the literature.^{2,35}

Considerable variation was found in the shape and height of the greater trochanter among all femurs and between groups. There were also large variations among femurs in the distance between the greater trochanter and the center of the head (i.e., femoral offset) and the neck diameter, demonstrating the utility of SSM for objectively describing variations in femoral shape and the spectrum of possible deformities, which would be difficult to identify using radiographs.

Mean shapes calculated using SSM and color plots of individual cam femurs compared to the mean shapes could be used to improve FAI diagnosis and treatment. For example, a 3D reconstruction of a patient with cam FAI could be objectively compared to the mean pathological shape to assess disease severity (relative to other cam patients), or could be compared to the mean control femur to produce a map elucidating the magnitude and location of bone debridement required to make the head normal in appearance (Fig. 6). Undercorrection of a cam lesion may cause lingering pain and could require revision surgery, while over correction could endanger the mechanical integrity or blood supply of the femur.^{36,37} 3D debridement maps from

objective SSM could facilitate more exact surgical planning.

A persistent problem with diagnosing cam FAI is the establishment of rubrics that can reliably distinguish pathologic from normal femurs. Along with quantifying the spectrum of deformities and variations between groups, we also demonstrated how SSM could be used to develop new, perhaps more reliable measurements of anatomy to diagnose FAI. For instance, SSM suggested that the distance between the greater and lesser trochanters was highly variable and different between groups. While these results are preliminary, the disparity in greater trochanter morphologies may indicate a developmental deformity at the trochanteric physis during early adolescence, concomitant with suggested capital femoral physal deformities.^{38,39}

Our results also suggest that femoral offset is largely variable in control and cam FAI subjects. This variability may contribute to susceptibility for FAI by reducing available clearance between the lateral acetabular rim and proximal neck during extreme ranges of motion. Differences in concavity of the neck were not appreciable in mode 1 for normal subjects over ± 2 SD (Fig. 5). However, in cam FAI patients, the concavity was substantially altered over ± 2 SD in mode 1 (compare shape of -2 SD to $+2$ SD in mode 1 for cam patients in Fig. 5). Considerable variability in the concavity of the head–neck junction likely contributes to the susceptibility for FAI.

PC loading values were significantly different between controls and patients for the first two modes. Therefore, variation captured within these modes may be the most useful for identifying shape alterations contributing to FAI rather than inherent femur population variance. Localized information on variation among control and cam femurs could help physicians classify unusual cases and characterize morphological variations that distinguish healthy and pathologic hips.

A strong correlation was found between alpha angles from the frog-leg lateral view and maximum deviations from a sphere, likely because these measures assume circular/spherical geometry. However, only moderate to weak correlative relationships were found between shape variations from SSM and existing 2D and 3D measures of femoral morphology. These relatively weak correlations suggest that current radiographic criteria may inadequately describe the underlying variation in anatomy in FAI patients. Radiographic measurements of cam FAI can only provide a single value to describe head shape or neck concavity separately (alpha angle, head neck offset, respectively), and therefore may not fully capture anatomical differences (Fig. 1). Still, radiographs will likely continue to serve as the primary means to diagnose cam FAI. It may be possible to relegate 3D SSM-derived data to 2D radiographs of an average normal/FAI subject. These data could serve as a

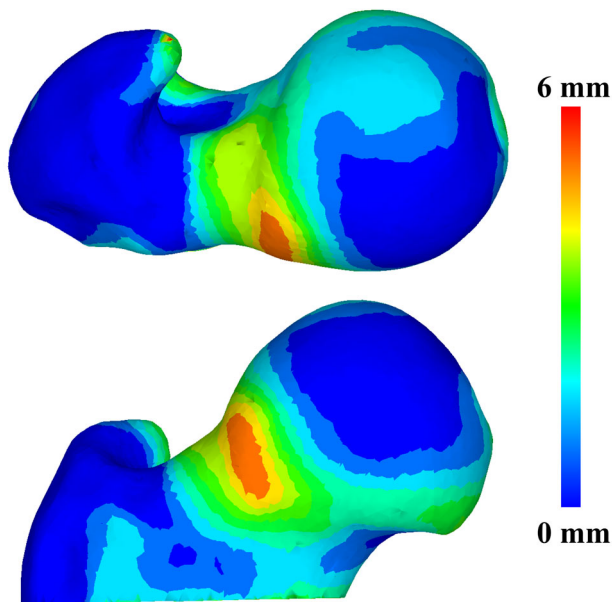


Figure 6. Color plot of a single cam FAI femur (shown) and the amount it deviated from the average control femur. These plots could be used as guide for planning surgical debridement to relieve FAI.

template to compare individual patient radiographs, or could be used to develop new radiographic measurements (e.g., those of the greater trochanter).

Recently, maximum deviation from a sphere has been compared between normal subjects and cam FAI patients.³⁴ Maximum deviation from a sphere may allow a more comprehensive examination of head out-of-roundness. For the patient modeled in Figure 6, maximum deviation was 6.6 mm, which is similar to maximum deviation between this patient and the group mean shape. However, measurements of 3D asphericity do not consider the width of the neck and height of the trochanter, which both varied substantially in the femurs of our study. Thus, in contrast to 3D measures of asphericity and 2D radiographic measurements, SSM allows for objective, 3D characterization of the entire proximal femur. Future research should determine if SSM is diagnostically superior to standard radiographic and 3D asphericity measurements.

Limitations of our study warrant discussion. First, some risk exists that control subjects could have had subtle forms of FAI. We used the most widely recognized radiographic measures of cam FAI (alpha angle from a lateral view and head-neck offset) to establish inclusion criteria. We also used three levels of exclusion criteria (evidence of osteoarthritis, gross bony deformities, alpha angle, and head-neck offset values outside previously reported ranges for asymptomatic subjects^{9,26}). Alpha angles, head-neck offsets, and 3D maximum deviations from a sphere were all significantly, and substantially, different between the control and cam FAI femurs; thus, we believe the two groups were distinct. Another limitation was that SSM was not applied to the acetabulum. In our study, a few patients were treated for chondrolabral damage on the acetabulum, which may have been caused by acetabular deformities. However, the primary diagnosis was cam-type FAI. Future research will include methods to consider both the femoral and acetabular sides of the hip joint simultaneously. Finally, alignment errors between femoral reconstructions could have affected SSM results. To reduce such errors, femoral reconstruction alignment was controlled using a strict relative RMS error stipulation, and the generalized Procrustes algorithm was applied during optimization, which assisted in removing any residual, non-shape information from the model.

In conclusion, we showed that SSM can differentiate anatomical differences in the shape of the proximal femur between cam FAI patients and control subjects. Our methodologies lay the groundwork for additional research and deployment of SSM as a clinical tool. Because of its objectivity, SSM could be used to stage disease severity (e.g., assign *z*-scores), which would be useful for patients who are symptomatic, but do not have obvious deformities. As a pre- or intra-operative surgical tool, SSM could be used to characterize the amount of bone that should be resected to restore

normal shape. Finally, SSM data could be used to identify novel anatomical variations between groups, which could in turn be used to develop more sensitive and specific measurements. Our SSM approach could be modified to output an average 'normal' and FAI radiograph that could be used as a template to efficiently diagnose patients.

ACKNOWLEDGMENTS

The authors acknowledge funding from the National Institutes of Health (R01-AR053344) and Dr. Hugh West Jr. of Intermountain Healthcare.

REFERENCES

1. Ganz R, Parvizi J, Beck M, et al. 2003. Femoroacetabular impingement: a cause for osteoarthritis of the hip. *Clin Orthop Relat Res* 417:112–120.
2. Beck M, Kalhor M, Leunig M, et al. 2005. Hip morphology influences the pattern of damage to the acetabular cartilage: femoroacetabular impingement as a cause of early osteoarthritis of the hip. *J Bone Joint Surg Br* 87:1012–1018.
3. Beaulé PE, Zaragoza E, Motamedi K, et al. 2005. Three-dimensional computed tomography of the hip in the assessment of femoroacetabular impingement. *J Orthop Res* 23:1286–1292.
4. Clohisy JC, Carlisle JC, Beaulé PE, et al. 2008. A systematic approach to the plain radiographic evaluation of the young adult hip. *J Bone Joint Surg Am* 90:47–66.
5. Rakhra KS, Sheikh AM, Allen D, et al. 2009. Comparison of mri alpha angle measurement planes in femoroacetabular impingement. *Clin Orthop Relat Res* 467:660–665.
6. Barton C, Salineros MJ, Rakhra KS, et al. 2011. Validity of the alpha angle measurement on plain radiographs in the evaluation of cam-type femoroacetabular impingement. *Clin Orthop Relat Res* 469:464–469.
7. Clohisy JC, Carlisle JC, Trousdale R, et al. 2009. Radiographic evaluation of the hip has limited reliability. *Clin Orthop Relat Res* 467:666–675.
8. Allen D, Beaulé PE, Ramadan O, et al. 2009. Prevalence of associated deformities and hip pain in patients with cam-type femoroacetabular impingement. *J Bone Joint Surg Br* 91:589–594.
9. Pollard TC, Villar RN, Norton MR, et al. 2010. Femoroacetabular impingement and classification of the cam deformity: the reference interval in normal hips. *Acta Orthop* 81:134–141.
10. Sutter R, Dietrich TJ, Zingg PO, et al. 2012. How useful is the alpha angle for discriminating between symptomatic patients with cam-type femoroacetabular impingement and asymptomatic volunteers? *Radiology* 264:514–521.
11. Peters CL, Erickson JA. 2006. Treatment of femoro-acetabular impingement with surgical dislocation and debridement in young adults. *J Bone Joint Surg Am* 88:1735–1741.
12. Almoussa S, Barton C, Speirs AD, et al. 2011. Computer-assisted correction of cam-type femoroacetabular impingement: a sawbones study. *J Bone Joint Surg Am* 93:70–75.
13. Audenaert EA, Baelde N, Huyse W, et al. 2011. Development of a three-dimensional detection method of cam deformities in femoroacetabular impingement. *Skeletal Radiol* 40:921–927.
14. Cates J, Fletcher PT, Styner M, et al. 2007. Shape modeling and analysis with entropy-based particle systems. *Inf Process Med Imaging* 20:333–345.
15. Cootes TF, Taylor CJ, Cooper DH, et al. 1995. Active shape models-their training and application. *Comput Vis Image Underst* 61:38–59.

16. Bredbenner TL, Eliason TD, Potter RS, et al. 2010. Statistical shape modeling describes variation in tibia and femur surface geometry between control and incidence groups from the osteoarthritis initiative database. *J Biomech* 43:1780–1786.
17. Bryan R, Mohan PS, Hopkins A, et al. 2010. Statistical modelling of the whole human femur incorporating geometric and material properties. *Med Eng Phys* 32:57–65.
18. Fitzpatrick CK, Baldwin MA, Laz PJ, et al. 2011. Development of a statistical shape model of the patellofemoral joint for investigating relationships between shape and function. *J Biomech* 44:2446–2452.
19. Blanc R, Seiler C, Szekely G, et al. 2012. Statistical model based shape prediction from a combination of direct observations and various surrogates: application to orthopaedic research. *Med Image Anal* 16:1156–1166.
20. Zheng G, Dong X, Rajamani KT, et al. 2007. Accurate and robust reconstruction of a surface model of the proximal femur from sparse-point data and a dense-point distribution model for surgical navigation. *IEEE Trans Biomed Eng* 54:2109–2122.
21. Barratt DC, Ariff BB, Humphries KN, et al. 2004. Reconstruction and quantification of the carotid artery bifurcation from 3-d ultrasound images. *IEEE Trans Med Imaging* 23:567–583.
22. Meller S, Kalendar WA. 2004. Building a statistical shape model of the pelvis. *ICS* 1268:561–566.
23. Davies RH, Twining CJ, Cootes TF, et al. 2002. A minimum description length approach to statistical shape modeling. *IEEE Trans Med Imaging* 21:525–537.
24. Harris MD, Anderson AE, Henak CR, et al. 2012. Finite element prediction of cartilage contact stresses in normal human hips. *J Orthop Res* 30:1133–1139.
25. Ruff CB, Hayes WC. 1988. Sex differences in age-related remodeling of the femur and tibia. *J Orthop Res* 6:886–896.
26. Clohisy JC, Nunley RM, Otto RJ, et al. 2007. The frog-leg lateral radiograph accurately visualized hip cam impingement abnormalities. *Clin Orthop Relat Res* 462:115–121.
27. Eijer H, Leunig M, Mahomed N, et al. 2001. Cross table lateral radiographs for screening of anterior femoral head-neck offset in patients with femoro-acetabular impingement. *Hip Int* 11:37–41.
28. Notzli HP, Wyss TF, Stoecklin CH, et al. 2002. The contour of the femoral head-neck junction as a predictor for the risk of anterior impingement. *J Bone Joint Surg Br* 84:556–560.
29. Anderson AE, Ellis BJ, Peters CL, et al. 2008. Cartilage thickness: factors influencing multidetector ct measurements in a phantom study. *Radiology* 246:133–141.
30. Datar M, Cates J, Fletcher PT, et al. 2009. Particle based shape regression of open surfaces with applications to developmental neuroimaging. *Med Image Comput Comput Assist Interv* 12:167–174.
31. Gower J. 1975. Generalized procrustes analysis. *Psychometrika* 40:33–51.
32. Franklin SB, Gibson DJ, Robertson PA, et al. 1995. Parallel analysis: a method for determining significant principal components. *J Veg Sci* 6:99–106.
33. Finner H. 1993. On a monotonicity problem in step-down multiple test procedures. *J Am Stat Assoc* 88:920–923.
34. Harris MD, Reese SP, Peters CL, et al. 2013. Three-dimensional quantification of femoral head shape in controls and patients with cam-type femoroacetabular impingement. *Ann Biomed Eng* 41:1162–1171.
35. Peters CL, Erickson JA, Anderson L, et al. 2009. Hip-preserving surgery: understanding complex pathomorphology. *J Bone Joint Surg Am* 91:42–58.
36. Mardones RM, Gonzalez C, Chen Q, et al. 2006. Surgical treatment of femoroacetabular impingement: evaluation of the effect of the size of the resection. *Surgical technique. J Bone Joint Surg Am* 88:84–91.
37. Philippon MJ, Schenker ML, Briggs KK, et al. 2007. Revision hip arthroscopy. *Am J Sports Med* 35:1918–1921.
38. Ogden JA. 1990. *Skeletal injury in the child*. Philadelphia, PA: W.B. Saunders Company.
39. Siebenrock KA, Wahab KH, Werlen S, et al. 2004. Abnormal extension of the femoral head epiphysis as a cause of cam impingement. *Clin Orthop Relat Res* 418:54–60.